RIVER RESEARCH AND APPLICATIONS

River Res. Applic. (2015)

Published online in Wiley Online Library
(wileyonlinelibrary.com) DOI: 10.1002/rra.2888

RIVER TEMPERATURE MODELLING BY STRAHLER ORDER AT THE REGIONAL SCALE IN THE LOIRE RIVER BASIN, FRANCE

A. BEAUFORT[a*], F. MOATAR[a], F. CURIE[a], A. DUCHARNE[b], V. BUSTILLO[c] AND D. THIÉRY[d]

[a] *EA 6293 GéHCO Géo-Hydrosystèmes Continentaux, Université François-Rabelais de Tours, Tours, France*
[b] *UMR 7619 Metis, Université Pierre et Marie Curie/CNRS, Paris, France*
[c] *CESBIO UMR 5126 (CNES-CNRS-IRD-UPS), IUT Paul Sabatier, Auch, France*
[d] *Bureau de Recherches Géologiques et Minières (BRGM), Orléans, France*

ABSTRACT

Daily water temperature was simulated at a regional scale during the summer period using a simplified model based on the equilibrium temperature concept. The factors considered were heat exchanges at the water/atmosphere interface and groundwater inputs. The selected study area was the Loire River basin (110 000 km^2), which displays contrasted meteorological, hydrological and geomorphological features. To capture the intra-basin variability of relevant physical factors driving the hydrological and thermal response of the system, the modelling approach combined a semi-distributed hydrological model, simulating the daily discharge at the outlet of 68 subwatersheds (drainage area between 100 and 3700 km^2), and a thermal model, simulating the average daily water temperature for each Strahler order in each subwatershed. Simulations at 67 measurement stations revealed a median root mean square error (RMSE) of 1.9°C in summer between 2000 and 2006. Water temperature at stations located more than 100 km from their headwater was adequately simulated (median RMSE < 1.5°C; −0.5°C < median biases < 0.5°C). However, performance for rivers closer to their source varied because of the averaging of geomorphological and hydrological features across all the tributaries with the same Strahler order in a subwatershed, which tended to mask the specific features of the tributaries. In particular, this increased the difficulty of simulating the thermal response of groundwater-fed rivers during the hot spells of 2003. This modelling by coupling subwatershed and Strahler order for temperature simulations is less time-consuming and has proven to be extremely consistent for large rivers, where the addition of streambed inputs is adequate to describe the effect of groundwater inputs on their thermal regime. Copyright © 2015 John Wiley & Sons, Ltd.

KEY WORDS: thermal model; daily river temperature; equilibrium temperature; Loire River; regional scale; Strahler order

Received 6 August 2014; Revised 28 January 2015; Accepted 10 February 2015

INTRODUCTION

River temperature is a major water quality parameter Most aquatic species have a specific range of water temperature that they can tolerate (Caissie, 2006), and a rise in temperature can affect the distribution of aquatic species (Tissot and Souchon, 2010). Many studies in river ecology use the air temperature as a proxy for the stream temperature to study the distribution of aquatic species given that water temperature records are often not available for all sampling sites (Tisseuil *et al*., 2012). Both temperature metrics are generally highly correlated (Buisson *et al*., 2008; Durance and Ormerod, 2009), but air temperatures may be a poor surrogate for stream temperatures in headwater reaches (Caissie, 2006). The river temperature modelling at a large catchment scale could help to overcome these inaccuracies and may constitute an important data source, which could be very useful for ecological studies.

River temperature is influenced by natural factors including atmospheric conditions, topography, riverine vegetation, river flow and heat fluxes at the riverbed/water interface (Caissie, 2006; Hannah *et al*., 2008; Webb *et al*., 2008) and by anthropogenic factors such as man-made levees (Bartholow *et al*., 2004), reservoirs (Poirel *et al*., 2009), warm-water input from wastewater (Kinouchi *et al*., 2007) and/or power plants (Bonnet *et al*., 2000) and forest clearing (Moore *et al*., 2005). Many modelling approaches have been implemented to describe the thermal regime of rivers divided into those that are data oriented, either statistical (Ducharne, 2008; Webb *et al*., 2003) or stochastic (Caissie *et al*., 2005), and those that are physically based. The physically based approach consists of solving the heat budget equation (Ouellet *et al*., 2014a; St-Hilaire *et al*., 2003) and can be complex as it can include all relevant heat fluxes at both the water surface and sediment/water interface (Herb and Stefan, 2011), and some models have been linked to hydrological models (van Vliet *et al*., 2013). It is therefore

*Correspondence to: A. Beaufort, Université François-Rabelais de Tours, EA 6293 GéHCO Géo-Hydrosystèmes Continentaux, Parc de Grandmont, 37200 Tours, France.
E-mail: aurelien.beaufort@univ-tours.fr

particularly suitable for climate change impact studies (Bustillo *et al*., 2014; van Vliet *et al*., 2013).

However, because of the amount and the complexity of data required, one-dimensional or two-dimensional deterministic thermal models are generally restricted to single-segment rivers or to small catchments (Carrivick *et al*., 2012; Loinaz *et al*., 2013; Ouellet *et al*., 2014b). To overcome these difficulties, several authors have proposed a simplified thermal model using the equilibrium temperature concept developed by Edinger *et al*. (1968); this is recognized to be an efficient way of simulating river temperature at the point scale (Bustillo *et al*., 2014; Caissie *et al*., 2005; Herb and Stefan, 2011). Most of these models are based on a classic heat budget equation accounting for five heat fluxes: net solar radiation, incoming long-wave atmospheric radiation, emitted long-wave radiation, air–water convection and evaporation/condensation (Bogan *et al*., 2003; Bustillo *et al*., 2014; Caissie *et al*., 2005). One model based on the equilibrium temperature concept, looking only at exchanges at the air–water interface, has shown excellent performance on the 250 km of the Middle Loire (Bustillo *et al*., 2014). However, groundwater–river exchanges may play an important role in the thermal regime of rivers, with major ecological implications (Hannah *et al*., 2004).

The main objective of this work is to assess the capacity of a simplified local thermal model, using the equilibrium temperature concept, to simulate the stream temperature of all tributaries contained in the Loire River Basin (110 000 km^2), which displays contrasted meteorological, hydrological and geomorphological features. The model takes into account six heat fluxes, including heat exchanges at the groundwater–river interface, based on the modified equilibrium temperature model that was successfully implemented by Herb and Stefan (2011) to estimate the thermal regime of cold-water stream reaches fed by groundwater. Modelling all 52 000 reaches forming the drainage network of the Loire River would be too costly in time needed for calculation. In that sense, our approach lies on the concept of stream order, used by Billen *et al*. (1994) in the RIVERSTRAHLER river quality model, which provides a generalized description of the morphology of drainage networks and which is less time-consuming. The evaluation was performed in summer (July–August) at 67 river temperature measurement stations. The daily discharge is simulated by a semi-distributed hydrological model at the outlet of 68 homogeneous subwatersheds (ranging from 100 to 3700 km^2) and constitutes an input data. For each Strahler order in a subwatershed, we applied the thermal model to the average reach, using geomorphological, meteorological and hydrological features averaged across all reaches with this Strahler order.

Thermal simulations considered forcing conditions by Strahler order and subwatershed and ignored advective processes that determine the upstream–downstream propagation of thermal signals. The testing period covered 7 years (2000–2006), during which time the Loire basin experienced a severe drought and very hot spells in August 2003. We assessed for what type of rivers the thermal model performed efficiently and where upstream conditions could be ignored. The adequacy of averaging the geomorphological and hydrological features at the Strahler order scale is discussed with regard to the thermal simulation performance, focusing particularly on river temperature in groundwater-fed streams during the hot spells of 2003.

STUDY SITE

The Loire River (Strahler order 8), the largest river in France, is 1020 km long and drains a 110 000-km^2 catchment area characterized by varied climate (oceanic and continental) and lithology (granites and basalts, sedimentary rocks, and granites and schist). The basin can be divided into three main areas (Figure 1a).

Area 1, mainly composed of granites, is a mountainous region with an average altitude of 800 m. The average slope of rivers in this area (12.4 m km^{-1}) is substantially higher than in areas 2 and 3 (3 and 4 m km^{-1}, respectively) (Table I). In headwater catchments (Strahler order ≤ 3), the average slope of streams is five times greater than those in areas 2 and 3. Above Strahler order 6, average slope is similar in all areas.

The major part of rivers in the basin has a pluvial regime, but several rivers located in area 1 have a pluvio-storm regime above 1500 m. Summer-specific flows, taken from the French HYDRO database (www.hydro.eaufrance.fr), have the same order of magnitude in each area, ranging from 4.2 L s^{-1} km^{-2} in area 1 to 2.5 L s^{-1} km^{-2} in area 3. However, looking at the ratio between the mean summer flow and the mean annual flow (Q_{JA}/Q_{Year}), we can see that the summer flow represents approximately 40% of the mean annual flow in area 2 but only 27% in area 1 and 20% in area 3 (Table I). This is consistent with the fact that area 2, composed of sedimentary rocks, benefits more from groundwater supplies in summer. This is even clearer for small rivers (Strahler order ≤ 3), in which the ratio is 50%, compared with 20% in other areas. The mean air temperature in summer, taken from the SAFRAN dataset, ranges from 18.2°C in the mountainous area to 20.5°C in lowland areas.

Stream shading is characterized by a vegetation cover indicator provided by the database of Valette *et al*. (2012). Rivers located in areas 1 and 2 have similar vegetation cover, 75% on average, for all Strahler orders, compared with only 35% in area 3 (Table I). However, for the smallest rivers (Strahler order ≤ 3), the mountainous area 1 has the greatest vegetation cover (~70%), compared with 65% in area 2 and 46% in area 3.

DOI: 10.1002/rra

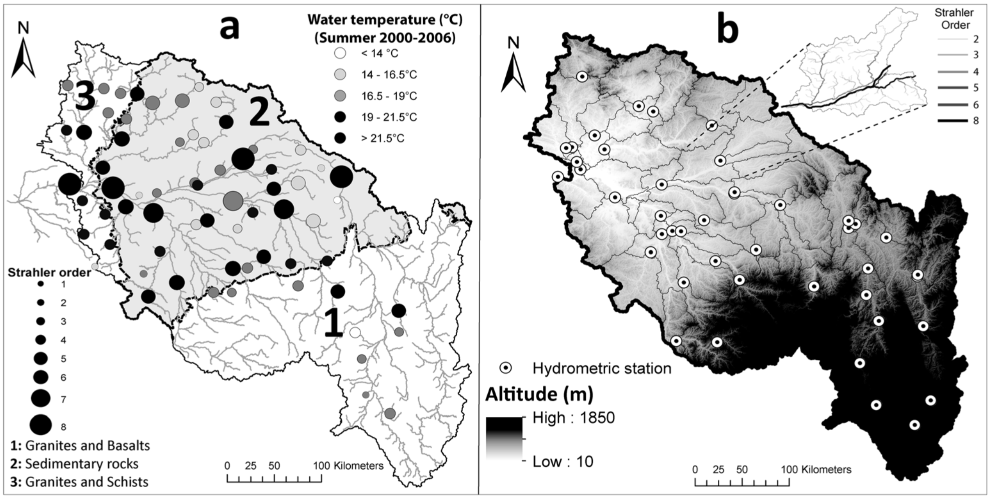

Figure 1. Map location of the 68 subwatersheds in the Loire River basin showing the main lithological areas and location of water temperature monitoring stations (a) and the delineation of the subwatersheds showing altitude and the location of hydrometric stations (b)

MODEL AND DATASETS

Equilibrium temperature concept

The thermal model is based on the heat balance approach and derived from the equilibrium temperature concept (Edinger *et al*., 1968), with two central variables, namely, the equilibrium temperature (T_e) and the heat exchange coefficient (K_e). The equilibrium temperature (T_e) is defined as the water temperature (T_w) at which the net rate of heat exchange at the limits of the water body, including the groundwater heat inflow, is zero. The thermal exchange coefficient (K_e) is the rate at which the water temperature responds to heat exchange processes ($\mathrm{W\,m^{-2}\,K^{-1}}$). Assuming that the river water is well mixed thermally, the heat budget equation of the water body can be expressed as follows:

$$\frac{\partial T_w}{\partial t} = \frac{\sum H_i(t)}{\rho_w C p_w D} \tag{1}$$

$$\sum_i H_i = H_{ns} + H_{la} - H_{lw} + H_c - H_e + H_g \tag{2}$$

where $\sum H_i$ is the net heat flux ($\mathrm{W\,m^{-2}}$), ρ_w is the water density ($1000\,\mathrm{kg\,m^{-3}}$), Cp_w is the specific heat of the water ($4181\,\mathrm{J\,kg^{-1}\,K^{-1}}$) and D is the mean river depth (m), which varies over time, like all heat fluxes ($\mathrm{W\,m^{-2}}$); H_{ns}

Table I. River characteristics by lithological area (1: granites and basalts; 2: sedimentary rocks; and 3: granites and schists) and Strahler order. Summer-specific flow Qs_{JA} (July–August) and ratio between mean summer flow Q_{JA} (July–August) and mean annual flow Q_{Year} are calculated for the period 1974–2006. Averaged vegetation cover on both sides of rivers with a buffer of 10 m is determined by remote sensing

		Order								
	Area	1	2	3	4	5	6	7	8	Mean
Slope ($\mathrm{m\,km^{-1}}$)	1	50.0	22.6	12.0	6.8	3.5	2.8	1.1	0.4	12.4
	2	10.0	5.2	2.8	1.7	1.4	1.2	1.0	0.5	3.0
	3	15.0	7.0	3.8	2.4	1.4	1.2	0.8	0.4	4.0
Qs_{JA} ($\mathrm{L\,s^{-1}\,km^{-2}}$) (hydrometric station available)	1	4.0 (11)		4.7 (23)		4.2 (25)		—		4.2
	2	3.6 (11)		3.8 (16)		3.8 (19)		3.0 (12)		3.6
	3	2.3 (2)		2.3 (8)		2.5 (11)		2.8 (2)		2.5
Ratio Q_{JA}/Q_{Year} (%)	1	23		27		30		—		27
	2	48		40		28		30		38
	3	9		15		20		28		19
Vegetation cover (%)	1	56	66	75	86	83	76	70	70	76
	2	53	60	69	78	85	82	84	75	73
	3	45	43	50	48	45	22	20	10	35

DOI: 10.1002/rra

is the net solar radiation, H_{la} is the atmospheric long-wave radiation, H_{lw} is the long-wave radiation emitted from the water surface, H_e is the evaporative heat flux, H_c is the convective heat flux exchanged with the atmosphere and H_g is the groundwater heat inflow. Their formulation (Table II) is taken from Bustillo *et al*. (2014) for the water atmosphere fluxes and from Herb and Stefan (2011) for the groundwater heat flux. The equilibrium temperature (T_e) is the temperature defined when the algebraic sum of the six heat fluxes is zero ($\sum H_i = 0$). This net heat flux can be linearized using the concept of equilibrium temperature (Edinger *et al*., 1968), stating that the net rate of heat exchange is proportional to the departure from the temperature equilibrium:

$$\sum_i H_i = K_e(T_e - T_w) \tag{3}$$

In line with Edinger *et al*. (1968), the heat exchange coefficient K_e was computed at the daily time step with a theoretical formulation corresponding to the sum of derivatives of heat fluxes with respect to water temperature (Bustillo *et al*., 2014), which does not require any calibration and is thus easily applicable at a regional scale:

$$\begin{aligned} K_e(t) = {} & 4\varepsilon\sigma(T_w(t) + 273.15)^3 \\ & + f(w)\left(0.62 + 6.11\frac{17.27\times 237.3}{(237.3 + T_w(t))^2}\right. \\ & \left.\times \exp\left[\frac{17.27\times T_w(t)}{237.3 + T_w(t)}\right]\right) + \rho_w C p_w \frac{Q_g(t)}{A} \end{aligned} \tag{4}$$

where *f*(*w*) is the wind function, taken from Brutsaert and Stricker (1979) (Table II), and Q_g/A defines the seepage flux (m s^{-1}). Next, the Edinger equation (combining Equations 1 and 3) was applied to compute K_e and T_e for solving the water temperature (T_w) at a daily time step:

$$\begin{aligned} T_w(t) = {} & T_e(t) \\ & + [T_w(t - \Delta t) - T_e(t)]\cdot\exp\left[\frac{-K_e(t)}{\rho_w C p_w D(t)}\Delta t\right] \end{aligned} \tag{5}$$

Implementation of the model at a regional scale

The local water temperature simulations were carried out in two stages (Figure 2). First, the equilibrium temperature (T_e)

Table II. Formulations and parameters used to determine heat fluxes occurring at the water/air and water/sediment interfaces (Brutsaert and Stricker, 1979; Bustillo *et al*., 2014; Sridhar *et al*., 2004)

Heat flux (W m^{-2})	Formulations	Parameters	Assumptions
Net solar radiation (H_{ns})	$H_{ns} = (1 - Alb)\cdot R_g \cdot (1 - SF)$	*Alb*: surface water albedo R_g: global radiation (W m^{-2}) *SF*: shading factor	$Alb = 0.06$
Long-wave radiation (H_{la})	$H_{la} = \varepsilon_a \cdot \sigma \cdot (T_a + 273.15)^4 \times (1 + 0.22 \cdot Cld^{2.75})$	ε_a: clear sky atmosphere emissivity σ: Boltzmann constant T_a: air temperature (°C) *Cld*: cloud cover fraction	ε_a = constant $\sigma = 5.67\times 10^{-8}$ W m^{-2} K^{-4}
Long-wave emitted radiation (H_{lw})	$H_{lw} = \varepsilon_w \cdot \sigma \cdot (T_w + 273.15)^4$	ε_w: water emissivity T_w: water temperature (°C)	$\varepsilon_w = 0.97$ $\sigma = 5.67\times 10^{-8}$ W m^{-2} K^{-4}
Convection (H_c)	$H_c = B \cdot f(w) \cdot (T_a - T_w)$	*B*: Bowen's coefficient $f(w) = aw + b$: wind function *w*: wind speed at 2 m (m s^{-1})	$a = 4$ W s m^{-3} mb^{-1} $b = 7.4$ W m^{-2} mb^{-1} $B = 0.62$ mb K^{-1}
Evaporation (H_e)	$H_e = f(w)\cdot(e_s - e_a)$	e_a: water vapour pressure in air (mb) e_s: saturation vapour pressure for T_w (mb)	Magnus–Tetens approximation: $e_s = 6.11\cdot\exp[(17.27\cdot T_w)/(237.3 + T_w)]$
Streambed inputs (H_g)	$H_g = \rho_w C p_w (Q_g/A)(T_g - T_w)$	T_g: groundwater temperature (°C) ρ_w: density of water (kg m^{-3}) Cp_w: specific heat capacity (J kg^{-1}°K^{-1}) Q_g: groundwater flow (m^3 s^{-1}) *A*: exchange area between groundwater and river (m^2)	

DOI: 10.1002/rra

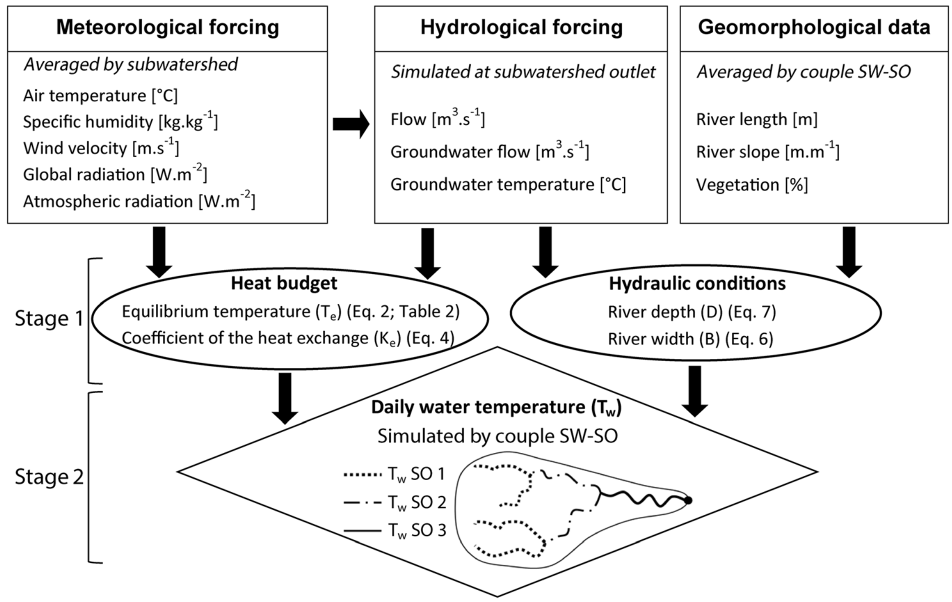

Figure 2. Principle of the model used to simulate daily water temperature at a regional scale. SW, subwatershed; SO, Strahler order

(Equation 3), the coefficient of heat exchange (K_e) (Equation 4) and the river depth (Equation 7) were calculated at a daily time step and for each subwatershed × Strahler order couple, hereafter called SW–SO (stage 1 in Figure 2). Second, the daily water temperature was computed using Equation 5. The Loire basin was subdivided into 68 subwatersheds (Figure 1b), with drainage areas ranging from 100 to 3700 km^2. Within each subwatershed, the maximum Strahler order varies between 5 and 8.

Meteorological forcing variables

Daily meteorological forcing data were taken from the SAFRAN dataset (Quintana-Seguí *et al*., 2008; Vidal *et al*., 2010), which was produced by Météo-France with an 8-km resolution for the period 1970–2007 at an hourly time step for the following near-surface parameters: air temperature (T_a, 2 m above ground level, °C), specific humidity (Q, 2 m above ground level, kg kg^{-1}), snowfall (S, mm s^{-1}), rainfall (R, mm s^{-1}), wind velocity (W, 10 m above ground level, m s^{-1}), global radiation (R_g, W m^{-2}) and atmospheric radiation (R_a, W m^{-2}). The wind velocity, measured 10 m above ground level, was extrapolated at a height of 2 m using a logarithmic wind profile, yielding $U_2/U_{10} = (2/10)^{0.11} = 0.837$, with 0.11 corresponding to the surface roughness of arable land (Zhang *et al*., 2004). Daily meteorological forcing data were spatially averaged for each subwatershed.

Geomorphological and vegetation data

The main characteristics (length and slope) of the drainage network were extracted from the CARTHAGE (Thematic cartography of the water agency and the French Ministry of Environment) database and the BD ALTI® 25-m resolution DTM dataset (IGN Paris, France). These characteristics were averaged for each SW–SO. Therefore, all river reaches with identical SO in an SW were assumed to share the same morphological features. River length was used to determine the exchange area between the river and the groundwater (A) for the calculation of the heat flux H_g, and the river slope was used to determine river depth (Equation 7) and width (Equation 6).

The river width (B) and depth (D) were determined at a daily time step using the ESTIMKART application, which takes into account the mean and daily flows of the reaches (Lamouroux *et al*., 2010), assuming a rectangular cross section:

$$B(t) = a_d \overline{Q}^{b_d} \left[Q(t) \overline{Q} \right]^b \tag{6}$$

$$D(t) = c_d \overline{Q}^{f_d} \left[Q(t) \overline{Q} \right]^f \tag{7}$$

where $\overline{Q}$ is the mean flow (m^3 s^{-1}), Q is the daily flow (m^3 s^{-1}), and b, f, a_d, b_d, C_d and f_d are coefficients and exponents, depending on river slope, watershed area and Strahler order. These parameters share common properties worldwide (Knighton, 1998; Lamouroux and Capra, 2002), and we used the formulations proposed by Lamouroux *et al*. (2010). River width was used to determine the exchange area (A) between the river and the groundwater for the calculation of the sixth heat flux (Table II), and river depth was included in the water temperature equation (Equation 5). The mean river width calculated using Equation 6 was compared with the width measured

DOI: 10.1002/rra

by aerial photography at 67 thermal measurement stations. The river width calculated is close to observations, the difference being less than 15%.

A shading factor (*SF*), corresponding to a coefficient of reduction of the overall incident radiation (H_{ns}), was determined from the database of Valette *et al*. (2012), which gives the averaged vegetation cover (%) determined by remote sensing on both sides of the rivers with a buffer of 10 m. The vegetation cover was averaged for each SW–SO and weighted linearly by a coefficient linked to the Strahler order, ranging from zero for a Strahler order 1 to one for a Strahler order 8, to account for the influence of river width on shading area. The shading factor is included in the net solar radiation equation (Table II).

Hydrological forcing variables

The daily mean discharge values ($m^3 s^{-1}$) were determined by the semi-distributed hydrological model EROS (Ecoulement dans une Rivière Organisée en Sous-bassins) (Thiéry, 1988; Thiéry and Moutzopoulos, 1995) at the outlet of the 68 subwatersheds, designed to be as homogeneous as possible with respect to land use and geology (Bustillo *et al*., 2014) (Figure 1b). Modelling the rainfall/discharge relationships entailed four to six lumped parameters (soil capacity, recession times, etc.) for each subwatershed. Runoff was assumed to be evenly distributed over each subwatershed, meaning that specific discharge, expressed in millimetres per day, is the same for all tributaries, whatever their Strahler order, provided they are located within the same subwatershed. Daily flows simulated at the outlet of a subwatershed were then redistributed in each SW–SO according to their drainage area. Simulations of daily mean discharge were performed over the period 1971–2007, using the meteorological forcing from the SAFRAN database. EROS was validated over the 1974–1999 period at 44 hydrometric stations of the 68 located at the outlet of subwatersheds with more than 20 years of time series (median drainage area: 3800 km^2; SO > 5) (Figure 1b). To test the performance of the hydrological model at medium and low flows, Nash criteria were calculated on the square roots of the discharge (C2) and the logarithms of the discharges (C3), providing a better assessment of performance in the low-flow period. Performance was good at the 44 hydrometric stations used for calibration with the C2 criterion between 0.84 and 0.87 and the C3 criterion between 0.77 and 0.95 in 75% of the subwatersheds during the low-water period (July–August), which is of particular interest for this study. However, they tend to be slightly overestimated at several stations, which can be explained by the fact that the hydrological model does not include water withdrawals for agriculture. This overestimation is greatest for specific flows higher than $4 l s^{-1} km^{-2}$ and can reach 40%. Looking at 87 intermediate stations (median drainage area: 320 km^2) located inside the subwatersheds and not at their outlet, the C3 criterion is higher than 0.7 in 40 stations. However, the performance is more contrasted, especially for stations located on small rivers (SO < 3) where the relative bias of simulated flows can reach ±60%.

To account for the influence of groundwater inputs on the thermal response of river reaches, we chose to add a sixth heat term (H_g), expressed in watts per square metre and corresponding to heat flux from streambed inputs (Herb and Stefan, 2011; Sridhar *et al*., 2004) and computed by SW–SO (Table II). The exchange area between the river and groundwater (*A*) corresponding to river length multiplied by wetted perimeter (m^2). The fraction of stream flow due to groundwater inputs was determined with base flow separation techniques based on the method of the Institute of Hydrology (1980) to obtain Q_g ($m^3 s^{-1}$). Because few techniques are available to estimate groundwater inflow temperature, T_g was estimated by averaging the air temperature of the 365 days preceding the observation according to Todd (1980). Heat transfer from the stream to the streambed sediment by conduction was ignored.

Water temperature data

The validation data consisted of daily mean river temperatures, computed from observed hourly data surveys performed at 67 stations (median drainage area = 350 km^2) managed by the Office National de l'Eau et des Milieux Aquatiques, mainly in summer between 2000 and 2006. These stations are not evenly distributed across the Loire basin (Figure 1a): 45 are in area 2, but only 10 in area 1 and 12 in area 3. They include all Strahler orders, although stations are principally located on medium-sized rivers with a Strahler order of 4 or 5 (38 stations). We can note that the highest mean summer temperatures are observed on large rivers such as the Loire and their main tributaries, where the mean water temperature in summer was over 21.5°C in 2000–2006. This period was marked by a severe drought in summer 2003 (1 in 50 years) and a hot spell (Moatar and Gailhard, 2006) with an increase of 3.2°C in the mean summer air temperature (T_a) compared with the 1974–2006 summer mean.

RESULTS

Multi-year evaluation. The model faithfully represents the water temperature observed at 67 measurement stations in summer between 2000 and 2006. The mean standard deviation of errors is 1°C and less than 0.5°C for five stations (Table III). The mean root mean square error (RMSE) is 2°C (Figure 3a). Biases ($T_{sim} - T_{obs}$) are small and range from −1°C to 1°C for 43 stations (65% of stations), as shown in Figure 3b. The model was most

DOI: 10.1002/rra

Table III. Air and water temperatures in summer (July–August) 2000–2006; average, minimum and maximum water temperatures observed (T_w-obs); average and maximum air temperatures (T_a); specific flow in summer (Qs_{JA}); and inter-summer performance of simulations at 67 measurement stations

	2000	2001	2002	2003	2004	2005	2006	2000–2006	1974–2006
T_w-obs mean (°C)	18.0	18.9	17.4	19.6	17.9	18.0	19.0	18.4	
T_w-obs max (°C)	21.9	22.7	21.8	25.3	22.4	22.3	23.8	22.9	
T_w-obs min (°C)	13.9	11.0	11.9	11.6	10.9	9.1	10.7	11.3	
T_a (°C)	18.4	19.4	18.2	22.1	19	19.2	20.3	19.7	18.9
T_a-max (°C)	23.1	24.2	22.6	27.7	23.5	24.2	25.1	24.3	25.6
Qs_{JA} (L s km^{-2})	4.1	5.1	2.9	2.1	3.6	1.9	2.0	3.1	3.5
Bias (T_w-sim − T_w-obs)	0.0	0.3	0.7	0.7	0.6	0.6	0.5	0.5	
Standard deviation of errors	1.0	1.1	1.2	1.3	1.1	1.2	1.2	1.2	
Root mean square error (°C)	1.6	1.5	2.1	2.4	2.1	2.1	2.2	2.0	

accurate for large rivers (Strahler orders 7 and 8), with biases ranging from −0.5°C to 0.5°C and a median RMSE of less than 1°C (large white circle; Figure 3a). For small streams with Strahler order equal to or less than 3, performance varied widely, with an average bias of 1.4°C and an average RMSE of 2.4°C, while RMSE was less than 1.5°C at five stations (small white and grey circle) and higher than 2.5°C at five stations (small black circle; Figure 3a). The average performance is improved as the distance from the source increased; for 16 stations located more than 100 km from their source (drainage area > 1000 km^2), the average standard deviation of errors was 0.8°C, compared with 1.3°C for the others (Figure 3c).

Inter-annual variability. The best performance for all stations was obtained in summer 2000 (RMSE = 1.6°C) and 2001 (RMSE = 1.5°C) with a bias close to zero (Table III). Average air and water temperatures for those 2 years were similar to the inter-summer mean (T_a = 19.7°C and T_w = 18.4°C, respectively), and their specific flows were slightly higher than the inter-annual mean. In 2004, 2005 and 2006, the performance was similar (RMSE = 2.1°C; bias = 0.6°C), and the average air temperature was close to the pluri-summer mean (T_a = 19.7°C). Summer was colder in 2002 (T_a = 18.2°C), but the performance was of the same order of magnitude as in 2004, 2005 and 2006.

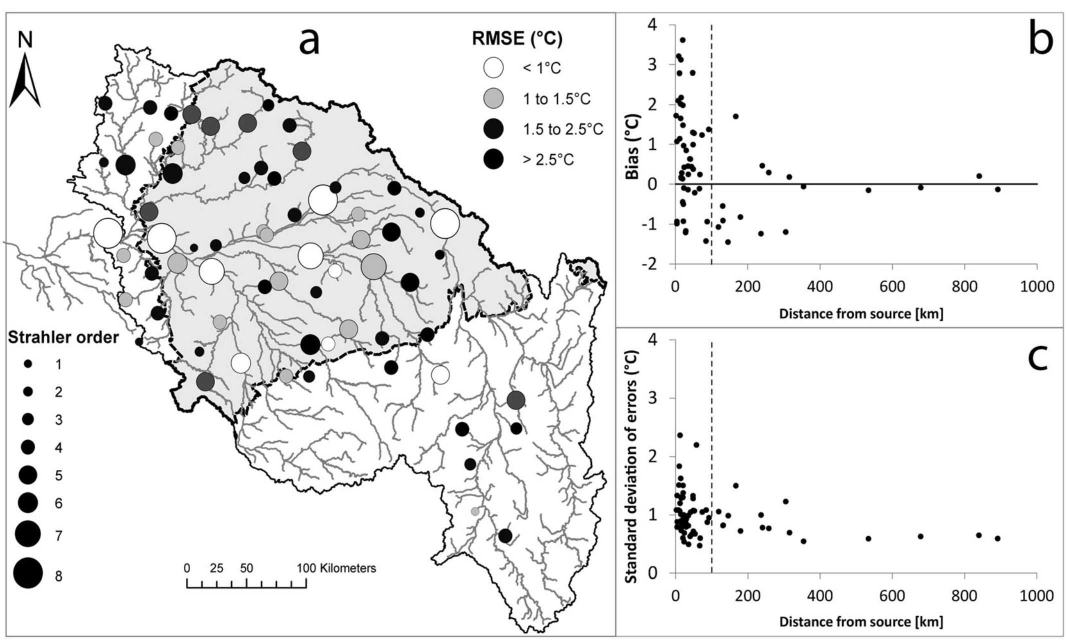

Figure 3. Thermal model performance at 67 measurement stations during the summer period between 2000 and 2006: (a) spatial distribution of root mean square error (RMSE), (b) biases ($T_{sim} - T_{obs}$) and (c) standard deviation of errors as a function of the distance from headwater

DOI: 10.1002/rra

The most poorly simulated summer was 2003, with overestimated water temperature (bias = 0.7°C) and an RMSE of 2.4°C. The average maximum daily temperature of air (T_a-max) observed at 67 sites was 2.1°C higher than the 1974–2006 summer mean, and the average specific flow was $1\,\mathrm{L\,s^{-1}\,km^{-2}}$ lower than the inter-summer mean (Table III). Despite this exceptional heat wave, the observed water temperature only increased by 1.2°C compared with the inter-summer mean. In fact, air warming was relatively homogeneous for all the sites, ranging from +2.5°C to +4°C, while the average water temperature variation was more contrasted (between −1°C and +4°C).

Sensitivity of the model. In this thermal model, several parameters, including groundwater flow (Q_g), river depth (D) and the shading factor (SF), remain difficult to quantify at the scale of a large regional watershed. To overcome these difficulties, we used empirical formulae as described in the first section of this paper. Here, we will examine the influence of these parameters on water temperature simulation.

The shading factor (ranging from 0 to 1) was included in the net solar radiation equation (Table II) and was used in the calculation of the equilibrium temperature (T_e). At the 67 measurement stations, increasing the shading factor by 50% lowered the average simulated water temperature by 4°C (Figure 4a) and tended to slightly decrease daily fluctuation of water temperature by 1.5°C (Figure 4d). Conversely, a 50% drop in the shading factor led to a 3°C rise in water temperature and a 1°C increase in the amplitude of water temperature fluctuation. The variation of the shading factor led to similar temperature changes in all the stations, which could be explained by the heterogeneous distribution of validation stations across the Loire basin. This was the most influential parameter in terms of temperature calculation (Figure 4g).

Groundwater flow ($\mathrm{m^3\,s^{-1}}$) was included in the streambed input equation constituting the sixth heat flux used to

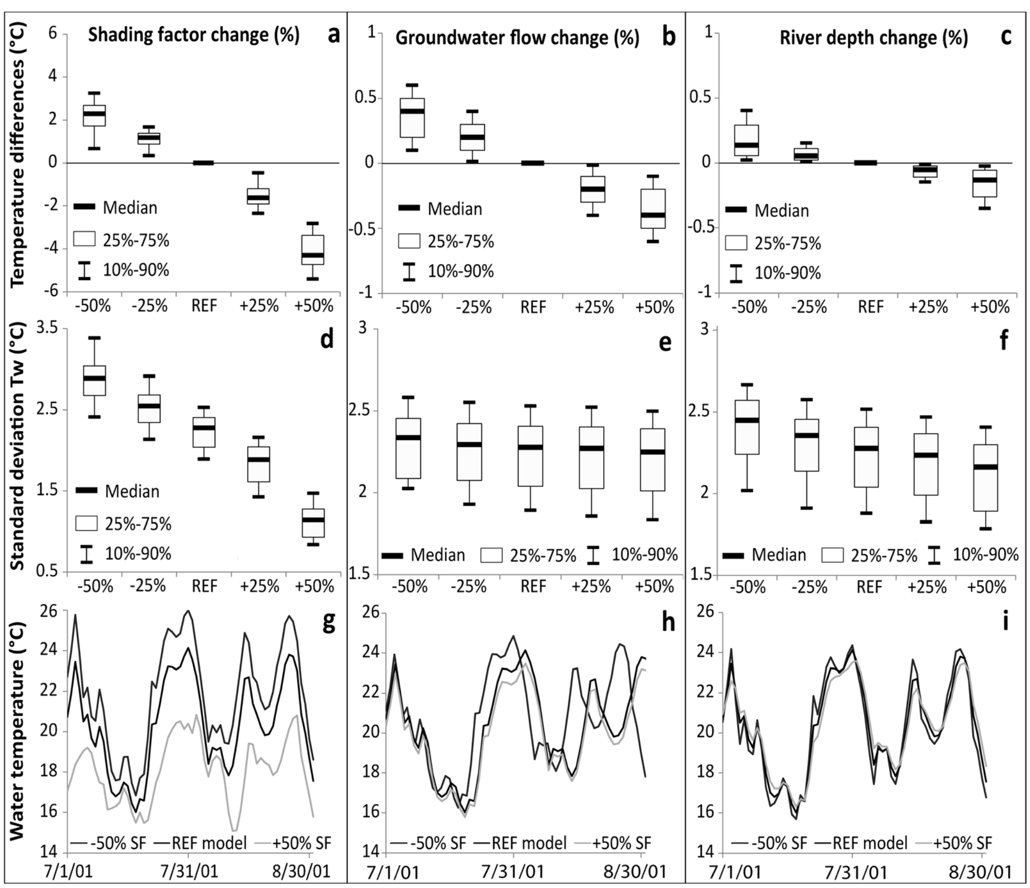

Figure 4. Model sensitivity: distribution of mean river temperature differences and water temperature variability with changes in shading factor (SF) (a, d), groundwater flow (Q_g) (b, e) and river depth (D) (c, f) at the 67 stations (whiskers) in summer 2000–2006. Example of temperature variations induced by changes in SF (g), G_w (h) and D (i) ranging from −50% (dashed grey line) to +50% (solid grey line) in a medium-sized river influenced by groundwater inputs (order 5; drainage area $750\,\mathrm{km^2}$) compared with daily temperature simulated by the reference model (described in the Model and Datasets section) in summer 2001 (solid black line)

DOI: 10.1002/rra

compute the heat budget (Table II). With a 50% increase in groundwater flow, the water temperature drops by 0.4°C during the summer period. Conversely, if the groundwater flow decreases by 50%, the water temperature rises by 0.4°C (Figure 4b). Groundwater flow has a buffering effect on the thermal regime of rivers, and a 50% increase can reduce the amplitude of water temperature fluctuation by 0.3°C. In summer, streambed inputs contribute to approximately 10% of the heat loss of the water body, which explains the low impact of changes in groundwater flow on the simulated water temperature. This value is similar to other studies (Hannah *et al*., 2008; Hebert *et al*., 2011). The most important temperature changes occurred for stations located in area 2, which benefit from a higher groundwater supply in summer. In a medium-sized river (Strahler order 5; drainage area 750 km^2) strongly influenced by groundwater flow, changes in temperature greater than 0.8°C may be observed (Figure 4h).

River depth (*D*) (Equation 2) was used in Equation 5 to calculate the water temperature and is one driver of the thermal inertia of the system. Its effect on mean summer temperature is very low (Figure 4f). However, a 50% increase in river depth led to an increase in thermal inertia, reducing the variability of the simulated daily temperature by 0.3°C (Figure 4i) at the 67 measurement stations. Conversely, a reduction of the river depth provoked a 0.3°C increase in the amplitude of variation of daily water temperature. Like for the shading factor, the variation of the river depth led to similar temperature changes in all the stations.

DISCUSSION

The model performance on large rivers is close to the RMSE value of 0.82°C calculated on the Loire River (Bustillo *et al*., 2014) but varied widely on small rivers close to their headwater. Mohseni and Stefan (1999) showed that after a long travel time, that is, a long distance from the headwater, the memory of the upstream temperature is lost, and weather is the main factor driving water temperature. For shorter travel times, local factors, including upstream water temperature and weather, determine the water temperature. When the station is very close to the headwater, that is, when the travel time is very short, the weather effect is small. Upstream water temperature may thus be colder (groundwater in summer and snowmelt) than the equilibrium water temperature determined by weather and local parameters. In this section, the importance of including geomorphological features, hydrological forcing variables and streambed inputs in the calculation of water temperature is discussed in relation to the thermal simulation performance.

Influence of geomorphological features

The thermal model is based on a simplifying assumption regarding the geomorphological features of rivers. In each SW–SO, we used the mean of the corresponding local values of river slope (*S*), river length (*L*) and shading factor (*SF*). Consequently, local geomorphological characteristics and riparian vegetation tended to be overlooked.

These parameters (*S*, *L* and *SF*) are assumed to be similar in rivers with the same Strahler order within a given subwatershed, giving rise to potential uncertainty regarding the water temperature simulation due to the heterogeneity of these features. To assess the magnitude of this uncertainty, we examined extreme values (minimum and maximum) of these three types of geomorphological feature for each instrumented SW–SO (67 stations) with the aim of estimating the potentially highest and lowest water temperatures. Two examples of this corresponding uncertainty range are displayed (Figure 5, grey area) around the water temperature simulated by the model (T_w-sim).

In these two rivers, with Strahler orders 7 and 4, the observed temperatures (T_w-obs) fall within the uncertainty area corresponding to geomorphological features variation. This suggests that averaging the geomorphological features has

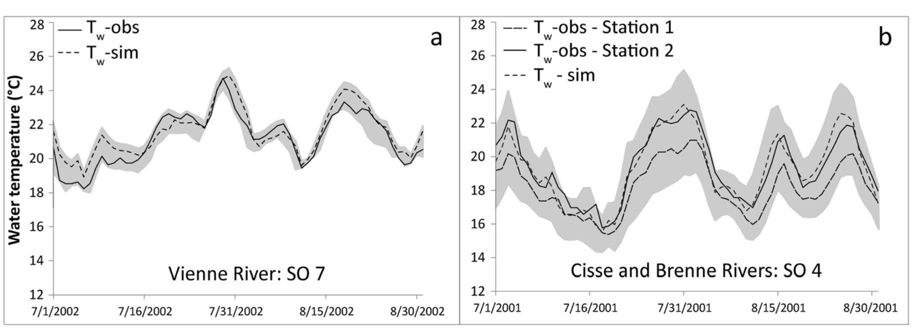

Figure 5. Daily observed and simulated water temperatures for two subwatershed–Strahler order (SO) couples. The grey area represents the simulation uncertainty linked to the averaging of geomorphological features: (a) the Vienne at Anché (Strahler order 7; 20 300 km^2) and (b) the Cisse at Noizay (station 1) and the Brenne at Chancay (station 2) (Strahler order 4; 350 km^2)

DOI: 10.1002/rra

a significant impact on the model; nevertheless, local simulations that are biased can be explained, in part, by this assumption. In one SW–SO, there are two measurement stations (Figure 5b), and we can see that the temperature simulated using average geomorphological features (T_w-sim) is closer to the temperature observed at station 2 (bias = 0.4°C; standard deviation of errors = 0.7°C) than at station 1 (bias = −0.9°C; standard deviation of errors = 0.9°C). However, the temperature curve at station 1 is included in the uncertainty area, suggesting that the lower performance observed at this station could be due to geomorphological forcing variables differing from the mean.

The uncertainty range is greater for temperatures simulated on small rivers close to their headwater. This is particularly apparent on the curve showing the longitudinal evolution of simulated summer temperatures along the Loire (Figure 6a). Near the headwaters, the specific geomorphological features of the Loire are averaged with those of other streams of Strahler order 1 in the same subwatershed. Because there are more small streams than large rivers in a subwatershed, the uncertainty area is larger when rivers are close to their headwater, up to 8°C for Strahler order 1. The uncertainty range 100 km downstream of the headwater (Strahler order 6) is only 1°C and remains constant up to the outlet (900 km), because there are fewer higher-order streams and thus less variability of geomorphological features. Regarding the monitoring stations located less than 100 km from the headwater, the variability of geomorphological features produces an average uncertainty in simulations of about 3.5°C for 51 stations (Figure 6b). The mean uncertainty concerning the remaining 16 stations (distance > 100 km from headwater) is 1°C. The mean observed water temperature in summer for 2000–2006 is still included in the uncertainty area except for six stations very close to their headwaters (<30 km) where simulated temperatures are sharply overestimated and cannot be explained only by the averaging of geomorphological features for each SW–SO.

Influence of hydrological forcing

Daily flows, used to determine river depth (Equation 7) and groundwater flow (Table II), are generally well simulated by EROS during the summer period at the outlet of 44 subwatersheds, but they tend to be slightly overestimated or underestimated (reaching ±60%) at most stations. These inaccuracies lead to overestimated or underestimated river depth, which plays an important role in the thermal inertia of rivers. Taking all measurement stations together, a flow change of ±60% leads to a ±25% change of river depth in summer (Equation 7). Nevertheless, a ±25% change of river depth can increase or decrease the standard deviation of the summer temperature by only 0.3°C (Figure 4) and has a limited effect on the daily water temperature simulated in summer.

The groundwater flow (Q_g) was obtained by base flow separation techniques (Institute of Hydrology, 1980). The base flow determined from simulated flows is 25% higher than the base flow determined from available observed flows in summer between 1974 and 2006. However, we saw that a 25% increase in base flow induced a decrease of only 0.2°C in the mean summer temperature.

The inaccuracies of simulated flows have an effect on the mean temperature and on the variability of daily temperature and might impair the performance of the model. However, these impacts are limited, and the overestimation of water temperature by more than 5°C at the six stations (Figure 6b) identified in the previous section, where T_w is clearly outside the uncertainty range related to the geomorphological heterogeneities, cannot only be explained by the quality of the daily flow simulation.

Integration of groundwater flow in the model

One of the aims of this work was to study the capacity of the model to simulate the thermal response of rivers preferentially fed by groundwater in summer. To this end, we focused on the 44 measurement stations located within the

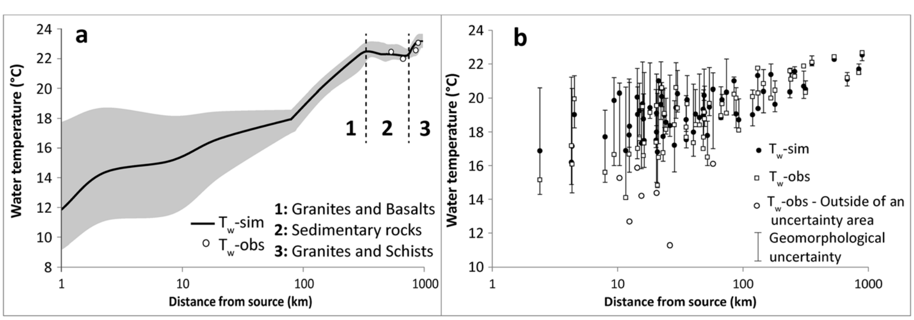

Figure 6. Mean water temperature simulated in summer between 2000 and 2006 as a function of distance from headwater: (a) longitudinal profile of temperature in the Loire River (geomorphological uncertainty in grey area) and (b) simulated and observed temperatures at 67 measurement stations

DOI: 10.1002/rra

sedimentary basin (Figure 1a; area 2) as they are the ones most influenced by groundwater inputs: the ratio observed between the mean summer flow and the mean annual flow (Q_{JA}/Q_{Year}) is 38% on average for all Strahler orders in area 2, compared with only 27% in area 1 and only 19% in area 3 (Table I).

The model simulates the average water temperature in summer very well, except for the six stations identified previously, where simulations are vastly overestimated (white circles; Figure 7a) with a bias of over 2.5°C (dashed line in Figure 7) and up to 7°C. These sites are close to their source (five sites < 20 km; one site 70 km from its source), and their mean observed water temperature is not included in the uncertainty range because of the averaging of geomorphological features (Figure 6b). The mean summer discharge observed at these stations represents approximately 55% of the mean annual flow, compared with only 30% for the other stations (Figure 7d). These rivers are not influenced by human activities or hydraulic management, so we can assume that they are largely sustained by groundwater inputs and that their thermal regime is cooled by the groundwater temperature. This is also suggested by the bias that is more important at these stations during the hot summer of 2003 (Figure 7c) than the cold summer of 2002 (Figure 7b), when it reached 11°C on rivers where the water temperature observed is usually cool (Figure 7c; white circles). Weather conditions have little influence on their thermal regime, and they maintained a relatively cool temperature over the entire period under study.

The model failed to simulate this particularity, because it underestimates groundwater cooling, which had a stronger influence during the heat wave of 2003, when the Q_g/Q ratio was larger. The groundwater temperature varies over a year but has a strong inertia, even during heat waves, which led to regulation of the thermal regime of rivers. In fact, the effect of groundwater inputs on the thermal regime of rivers in the Loire basin is described adequately by the sixth heat flux, except for these six stations. For example, in the middle Loire, 650 km from the headwater, Moatar and Gailhard (2006) observed a cooling of 1.4°C in August between 1980 and 2003, associated with a 10-m^3 s^{-1} groundwater inflow. A decrease of 0.8°C, but in July–August, is clearly simulated on the longitudinal profile of the Loire (Figure 6a) where the river crosses the area composed of sedimentary rocks and is fed by the Beauce aquifer (area 2). However, on small rivers, the groundwater flow and the exchange area between the river and the groundwater (A) are averaged for each SW–SO. In a real case, two rivers with the same SW–SO can have a very different groundwater flow or exchange area, and groundwater–river exchanges can be very complex and have a strong influence on their thermal regime (Hannah *et al*., 2009). Tonina and Buffington (2009) showed that the rate and area of groundwater exchanges vary as a function of the geomorphological features of rivers, which our model can only consider at the SW–SO scale. The implementation of a thermal model at a finer scale, including a definition of local geomorphological, hydrological and groundwater–river exchanges for each reach, could

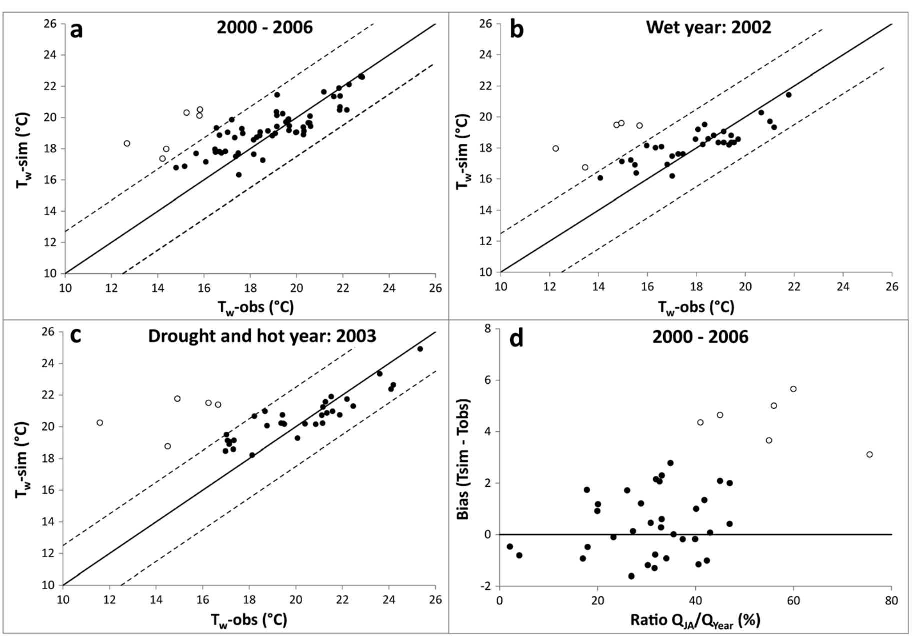

Figure 7. Simulated temperature as a function of observed temperature in summer 2000–2006 (a), in 2002 (b) and in 2003 (c). Dashed lines represent biases of ±2.5°C; (d) mean biases as a function of the ratio between the mean summer flow and the mean annual flow (Q_{JA}/Q_{Year}) in summer between 2000 and 2006 (white circle: stations where T_w-obs is outside the uncertainty area; black circle: other stations)

DOI: 10.1002/rra

greatly improve the thermal simulation of rivers, particularly those close to their source and largely fed by groundwater, as at the six stations described here.

The model is very efficient for rivers with low groundwater supplies and influenced mainly by weather conditions during heat waves (Figure 7c), especially those that are most impacted by warming ($T_w > 20°C$), and it can offer an appealing way to study the thermal response of rivers to climate change.

CONCLUSION

The main objective of this study was to assess the capacity of a simplified physically based model to simulate the spatiotemporal variability of river temperature in summer at a regional scale (110 000 km^2). According to the equilibrium temperature concept, river temperature is driven by local forcing conditions, and the upstream–downstream propagation of the thermal signal was not included. General performance at 67 measurement stations was good, with a mean RMSE of 1.9°C and a median bias of 0.7°C. The main conclusion is that the water temperature at stations located more than 100 km from their headwater is adequately simulated (mean RMSE < 1.5°C; −0.5°C < mean biases < 0.5°C). The good performances observed at these sites show that upstream conditions have a limited influence on the thermal regime of large rivers, and our discretization for temperature simulations by SW–SO is relevant for large rivers.

Performance on small rivers is more varied, partly because of the averaging of geomorphological features by SW–SO. Indeed, there is considerable geomorphological variability (river slope, river length and riparian vegetation) for small rivers inside a subwatershed. The uncertainty of simulations due to geomorphological averaging is greater on small rivers than on rivers with a high Strahler order (Figure 5). This averaging of geomorphological features tends to hide specific features of rivers and can explain poor local simulation of water temperature. Furthermore, daily flows, simulated by the EROS hydrological model, show good performance at the outlet of 44 subwatersheds in summer, but several intermediate stations are not very well simulated because of the simplifying hypothesis of homogeneous flow redistribution by SW–SO.

Another conclusion regards the efficiency of the integration of a sixth heat flux corresponding to streambed inputs, as shown in the longitudinal profile of the Loire (Figure 6a), except at six stations where the simulated temperatures are considerably overestimated, with mean biases of more than 2.5°C in summer (Figure 7a). These stations, located on small Strahler order streams, are largely fed by groundwater, and the difficulty in simulating the thermal response of rivers that are fed by groundwater in summer, especially during hot spells, seems to be linked to the groundwater flow and the exchange area between the river and the groundwater (A), which were averaged for each SW–SO. Like for the aforementioned geomorphology, the difficulty comes from assuming similar average features at the SW–SO scale.

To overcome these inaccuracies and improve simulations, a thermal model based on the local geomorphological and hydrogeological features of each reach should be implemented, and the number of subwatersheds used for the discharge simulation should be increased, so that heterogeneities in forcing conditions can be described at a finer scale. A better definition of the geomorphological and hydrological features of each reach, together with groundwater–river exchanges, could help identify rivers exhibiting a specific thermal response (low water temperature in summer) and offering favourable habitats or thermal refuge for cold-water fish species.

ACKNOWLEDGEMENTS

This work was realized in the course of work for a thesis funded by the Office National de l'Eau et des Milieux Aquatiques (ONEMA). It also benefitted from financial supports by the Fonds Européen de développement Régional, the Etablissement Public Loire and the water Agency of Loire Bretagne. Thanks are due to Météo-France for the SAFRAN database and to André Chandesris, Yves Souchon and Laurent Valette for the vegetation cover indicator database from the Institut national de recherche en sciences et technologies pour l'environnement et l'agriculture (IRSTEA) and the ONEMA.

REFERENCES

Bartholow JM, Campbell SG, Flug M. 2004. Predicting the thermal effects of dam removal on the Klamath River. *Environmental Management* **34**(6): 856–874. DOI: 10.1007/s00267-004-0269-5.

Billen G, Garnier J, Hanset Ph. 1994. Modelling phytoplankton development in whole drainage networks: the 'RIVERSTRAHLER' model applied to the Seine river system. *Hydrobiologia* **289**: 119–137.

Bogan T, Mohseni O, Stefan HG. 2003. Stream temperature–equilibrium temperature relationship. *Water Resources Research* **39**(9): 1245.

Bonnet M, Poulin M, Devaux J. 2000. Numerical modelling of thermal stratification in a lake reservoir: methodology and case study. *Aquatic Sciences* **62**: 105–124.

Brutsaert W, Stricker H. 1979. An advection–aridity approach to estimate actual regional evapotranspiration. *Water Resources Research* **15**: 443–450.

Bustillo V, Moatar F, Ducharne A, Thiéry D, & Poirel A. 2014. A multimodel comparison for assessing water temperatures under changing climate conditions via the equilibrium temperature concept: case study of the Middle Loire River, France. *Hydrological Processes* **28**: 1507–1524. DOI: 10.1002/hyp.9683.

Buisson L, Thuiller W, Lek S, Lim P, Grenouillet G. 2008. Climate change hastens the turnover of stream fish assemblages. *Global Change Biology* **14**: 2232–2248.

Caissie D, Satish MG, El-Jabi N. 2005. Predicting river water temperatures using the equilibrium temperature concept with application on Miramichi River catchments (New Brunswick, Canada). *Hydrological Processes* **19**: 2137–2159.

Caissie D. 2006. The thermal regime of rivers: a review. *Freshwater Biology* **51**: 1389–1406.

Carrivick JL, Brown LE, Hannah DM, Turner AGD. 2012. Numerical modelling of spatio-temporal thermal heterogeneity in a complex river system. *Journal of Hydrology* **414–415**: 491–502.

Ducharne A. 2008. Importance of stream temperature to climate change impact on water quality. *Hydrology and Earth System Sciences* **12**: 797–810.

Durance I, Ormerod SJ. 2009. Climate change effects on upland stream macroinvertebrates over a 25-year period. *Global Change Biology* **13**: 942–957.

Edinger JE, Duttweiler DW, Geyer JC. 1968. The response of water temperature to meteorological conditions. *Water Resources Research* **4**(5): 1137–1143. DOI: 10.1029/WR004i005p01137.

Hannah DM, Malcolm IA, Soulsby C, Youngson AF. 2004. Heat exchanges and temperatures within a salmon spawning stream in the Cairngorms, Scotland: seasonal and sub-seasonal dynamics. *River Research and Applications* **20**: 635–652.

Hannah DM, Malcolm IA, Soulsby C, Youngson AF. 2008. A comparison of forest and moorland stream microclimate, heat exchanges and thermal dynamics. *Hydrological Processes* **22**: 919–940.

Hannah DM, Malcolm IA, Bradley C. 2009. Seasonal hyporheic temperature dynamics over riffle bedforms. *Hydrological Processes* **23**: 2178–2194.

Hebert C, Caissie D, Satish MG, El-Jabi N. 2011. Study of stream temperature dynamics and corresponding heat fluxes within Miramichi River catchments (New Brunswick, Canada). *Hydrological Processes* **25**: 2439–2455. DOI: 10.1002/hyp.8021

Herb WR, Stefan HG. 2011. Modified equilibrium temperature models for cold-water streams. *Water Resources Research* **47**: W06519. DOI: 10.1029/2010WR009586

Institute of Hydrology. 1980. Low flow studies. Institute of Hydrology Research Report 1. Wallingford, UK: Institute of Hydrology.

Kinouchi T, Yagi H, Miyamoto M. 2007. Increase in stream temperature related to anthropogenic heat input from urban wastewater. *Journal of Hydrology* **335**: 78–88. DOI: 10.1016/j.jhydrol.2006.11.002 Mackey

Knighton D. 1998. Fluvial Forms and Processes: A New Perspective. John Wiley and Sons, New York, NY; 167–186.

Lamouroux N., Capra H. 2002. Simple predictions of instream habitat model outputs for target fish populations. *Freshwater Biology* **47**: 1543–1556.

Lamouroux N, Pella H, Vanderbecq A, Sauquet E & Lejot J. 2010. Estimkart 2.0: une plate-forme de modèles écohydrologiques pour contribuer à la gestion des cours d'eau à l'échelle des bassins français. Version provisoire. Cemagref—Agence de l'Eau Rhône-Méditerranée-Corse—Onema210.

Loinaz MC, Davidsen HK, Butts M, Bauer-Gottwein P. 2013. Integrated flow and temperature modeling at the catchment scale. *Journal of Hydrology* **495**: 238–251.

Moatar F, Gailhard J. 2006. Water temperature behaviour in the River Loire since 1976 and 1881. *Comptes Rendus Geoscience* **338**: 319–328.

Mohseni O, Stefan HG. 1999. Stream temperature/air temperature relationship: a physical interpretation. *Journal of Hydrology* **218**: 128–141.

Moore RD, Spittlhouse DL, Story A. 2005. Riparian microclimate and stream temperature response to forest harvesting: a review. *Journal of the American Water Resources Association* **41**: 813–834.

Ouellet V, Secretan Y, St-Hilaire A, Morin J. 2014a. Water temperature modelling in a controlled environment: comparative study of heat budget equations. *Hydrological Processes* **28**: 279–292. doi: 10.1002/hyp.9571

Ouellet V, Secretan Y, St-Hilaire A, Morin J. 2014b. Daily averaged 2D water temperature model for the St. Lawrence River. *River Research and Applications* **30**: 733–744. doi: 10.1002/rra.2664

Poirel A, Gailhard J, Capra H. 2009. Influence de la gestion des barrages- réservoirs sur la température de l'eau. Exemple d'application au bassin versant de l'Ain. Proceedings SHF: Etiages, Sécheresses, Canicules rares, et leurs impacts sur les usages de l'eau. 8–9 Octobre 2009, Lyon, 8 p.

Quintana-Seguí P, Le Moigne P, Durand Y, Martin E, Habets F, Baillon M, Canellas C, Franchisteguy L, Morel S. 2008. Analysis of near surface atmospheric variables: validation of the SAFRAN analysis over France. *Journal of Applied Meteorology and Climatology* **47**: 92–107. DOI: 10.1175/2007JAMC1636.1

Sridhar V, Sansone AL, LaMarche J, Dubin T, Lettenmaier DP. 2004. Prediction of stream temperature in forested watersheds. *Journal of the American Water Resources Association* **40**: 197–213.

St-Hilaire A, Morin G, El-Jabi N, Caissie D. 2003. Sensitivity analysis of a deterministic water temperature model to forest canopy and soil temperature in Catamaran Brook (New Brunswick, Canada). *Hydrological Processes* **17**: 2033–2047.

Thiéry D. 1988. Forecast of changes in piezometric levels by a lumped hydrological model. *Journal of Hydrology* **97**: 129–148.

Thiéry D, Moutzopoulos C. 1995. Un modèle hydrologique spatialisé pour la simulation de très grands bassins: le modèle EROS formé de grappes de modèles globaux élémentaires. In: VIIIèmes journées hydrologiques de l'ORSTOM "Régionalisation en hydrologie, application au développement", Le Barbé et E. Servat (Eds.), ORSTOM Editions; 285–295.

Tisseuil C, Leprieur F, Grenouillet G, Vrac M, Lek S. 2012. Projected impacts of climate change on spatio-temporal patterns of freshwater fish beta diversity: a deconstructing approach. *Global Ecology and Biogeography* **21**: 1213–1222.

Tissot L, Souchon Y. 2010. Synthèse des tolérances thermiques des principales espèces de poissons des rivières et fleuves de plaine de l'ouest européen. *Hydroécologie Appliquée* **17**: 17–76.

Todd DK. 1980. Groundwater Hydrology. John Wiley, Hoboken, N. J..

Tonina D, Buffington JM. 2009. Hyporheic exchange in mountain rivers I: mechanics and environmental effects. *Geography Compass* **3**(3): 1063–1086.

Valette L, Piffady J, Chandesris A, Souchon Y. 2012. SYRAH-CE: description des données et modélisation du risque d'altération de l'hydromorphologie des cours d'eau pour l'Etat des lieux DCE. Rapport final, Pôle Hydroécologie des cours d'eau Onema–Irstea Lyon, MALY-LHQ, juillet 2012; 104.

van Vliet MTH, Franssen WSP, Yearsley JR, Ludwig F, Haddeland I, Lettenmaier DP, Kabat P. 2013. Global river discharge and water temperature under climate change. *Global Environmental Change* **23**: 450–464. DOI: 10.1016/j.gloenvcha.2012.11.002

Vidal JP, Martin E, Franchistéguy L, Baillon M, Soubeyroux JM. 2010. A 50-year high-resolution atmospheric reanalysis over France with the Safran system. *International Journal of Climatology* **30**(11): 1627–1644.

Webb BW, Clack PD, Walling DE. 2003. Water–air temperature relationships in a Devon river system and the role of flow. *Hydrological Processes* **17**: 3069–3084. DOI: 10.1002/hyp.1280

Webb BW, Hannah DM, Dan Moore R, Brown LE, Nobilis F. 2008. Recent advances in stream and river temperature research. *Hydrological Processes* **22**: 902–918. DOI: 10.1002/hyp.6994

Zhang CL, Zou XY, Gong JR, Liu LY, Liu YZ. 2004. Aerodynamic roughness of cultivated soil and its influences on soil erosion by wind in a wind tunnel. *Soil and Tillage Research* **75**: 53–59